Electronic Supplementary Information

Thin Water Films and Magnesium Hydroxide Fiber Growth

by

Amir Gheisi†, Andreas Sternig†, Günther J. Redhammer§, Oliver Diwald*§

† Institute of Particle Technology, Universität Erlangen-Nürnberg, Germany
§ Department of Materials Science and Physics, Paris-Lodron University Salzburg, Austria

1) Electron microscopy

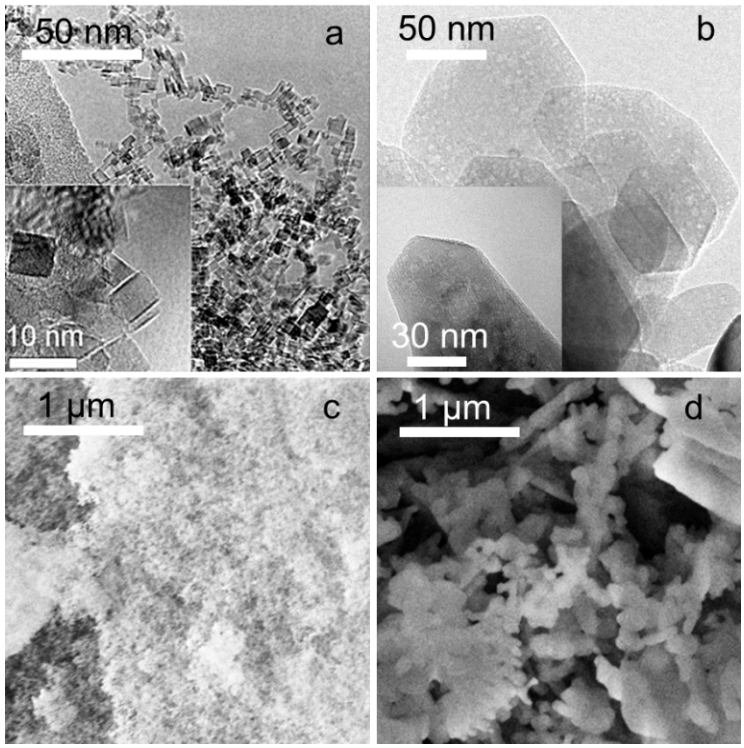

Figure S1: TEM images of a) MgO nanocube powders obtained by CVS and b) commercial MgO nanoparticles as reference material. SEM images of c) CVS MgO and d) commercial MgO nanoparticles. All images were taken after oxidation (T = 1123 K, p = 10 mbar O_2) and vacuum annealing (T = 1173 K, p < 5 x 10^{-6} mbar).

Transmission Electron Microscopy clearly shows that CVS MgO is characterized by agglomerates of highly dispersed monocrystalline nanocubes with a high portion of edge and corner features (Figure S1a). In contrast to MgO nanocubes, commercial MgO can be characterized as an assembly of less regular shaped particles (Figure S1b).

2) Powder X-ray Diffraction

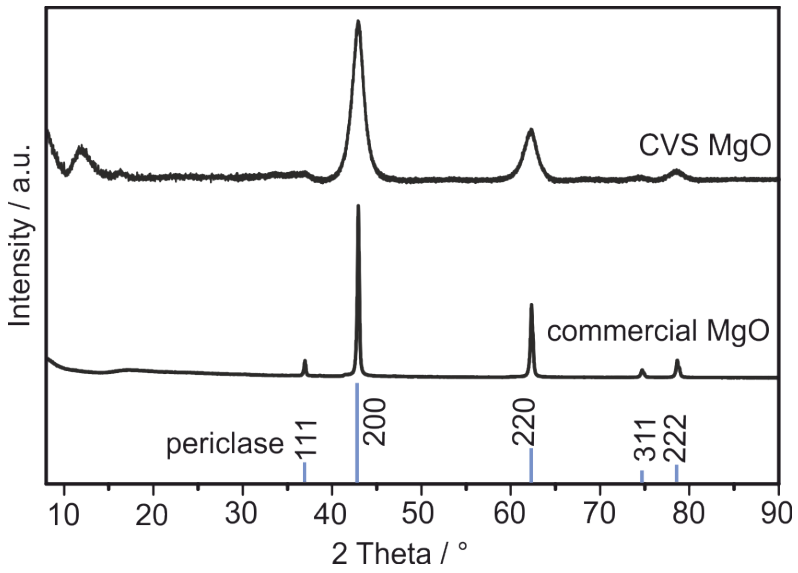

Figure S2: Powder XRD patterns of CVS MgO and commercial MgO nanoparticle powders after oxidation (T = 1123 K, p = 10 mbar O_2) and vacuum annealing (T = 1173 K, p < 5 $\cdot 10^{-6}$ mbar). The diffractograms clearly reveal that both particle types adopt crystal structures of the cubic phase. (Diffraction peaks indicating 2θ positions for the periclase structure are indicated as bars.)

3) Estimated surface coverages of $SiCl_4$/ O_2 on nanocrystalline MgO samples

Table S1 lists surface area of MgO powder samples, the estimated number of active surface sites, number of molecules supplied at a given pressure, monolayer equivalents (MLE, i.e. molecules provided to achieve a monolayer coverage at a sticking coefficient of S = 1) and incident molecular flux of $SiCl_4$ and O_2 per cycle. The gas properties are measured at 298 K considering the volume and other conditions of gas reservoir before exposure.

Table S 1: MgO sample weight, surface area and active sites available during the exposure experiment. Pressure, number of molecules, monolayer equivalent (MLE) and incident molecular flux of $SiCl_4$ and O_2 provided during one cycle.

				$SiCl_4$/ cycle				O_2 / cycle	
	weight (mg)	surface area (m^2)	Est. number of active sites* (m^{-2})	pressure (mbar) at RT	number of provided molecules	MLE (%)	incident flux of molecules (m^{-2} s^{-1})	pressure (mbar) at RT	incident flux of molecules (m^{-2} s^{-1})
CVS MgO	200	60	1.8	300	3×10^{21}	118	$1 \cdot 10^{27}$	700	$6 \cdot 10^{27}$
commercial MgO	200	2.5	<< 1	300	3×10^{21}	2832	$1 \cdot 10^{27}$	700	$6 \cdot 10^{27}$

*. According to a previous study the estimated number of active sites (corners and edges) corresponds to roughly 3% of the total surface area available.

4) XRD Phase Analysis of Reaction Products after contact of CVS MgO with $SiCl_4$ at RT

The quantitative phase analysis – with a good quality of refinement is good (e.s.d. of wt% ~1 %) - is demonstrated in **Figure S3**.

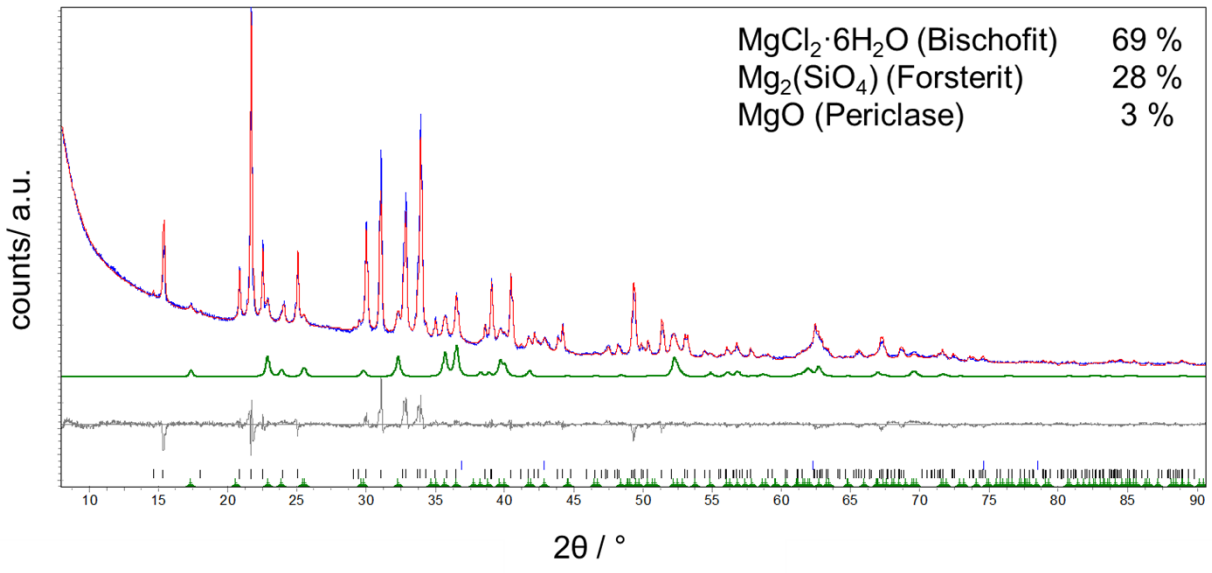

Figure S3: XRD pattern and results of the phase analysis for the same powder indicated in Figure 2 as fraction c2 and obtained after CVS MgO exposure to $SiCl_4/O_2$ at room temperature.

5) Experiments with commercial MgO

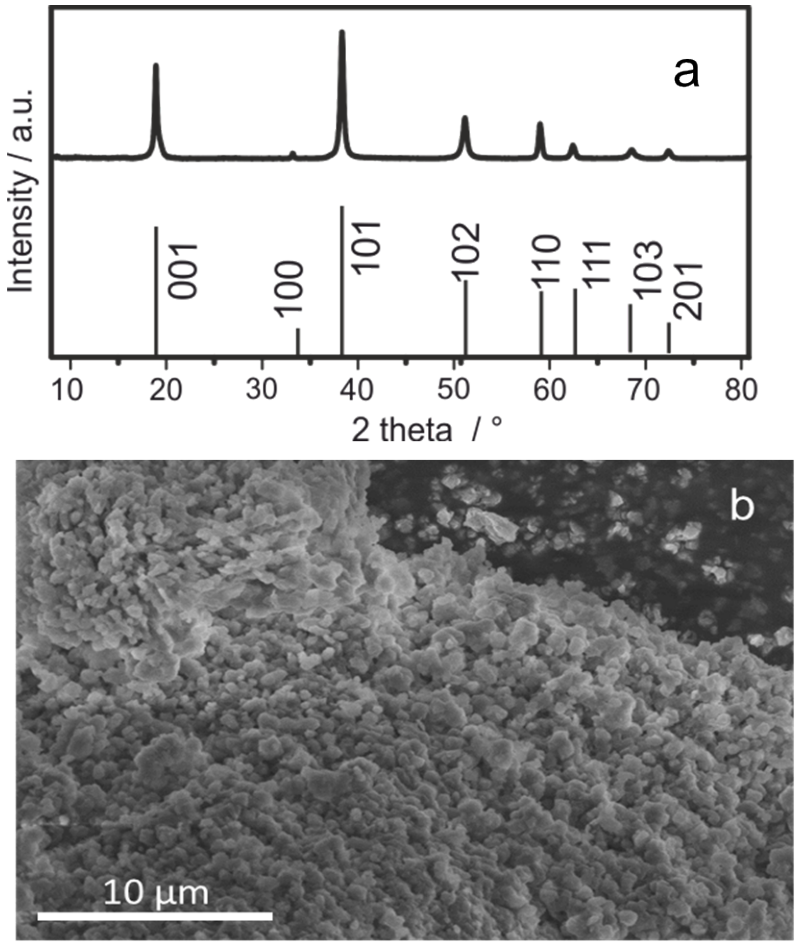

Figure S4: Commercial MgO after exposure to $SiCl_4/O_2$ and subsequent exposure to water-saturated air ($p(H_2O)$ = 32 mbar): a) Powder XRD pattern revealing the exclusive existence of brucite $Mg(OH)_2$; b) SEM image.

6) XRD phase analysis of the pattern measured after room temperature contact of surface functionalized MgO nanocubes with water vapor

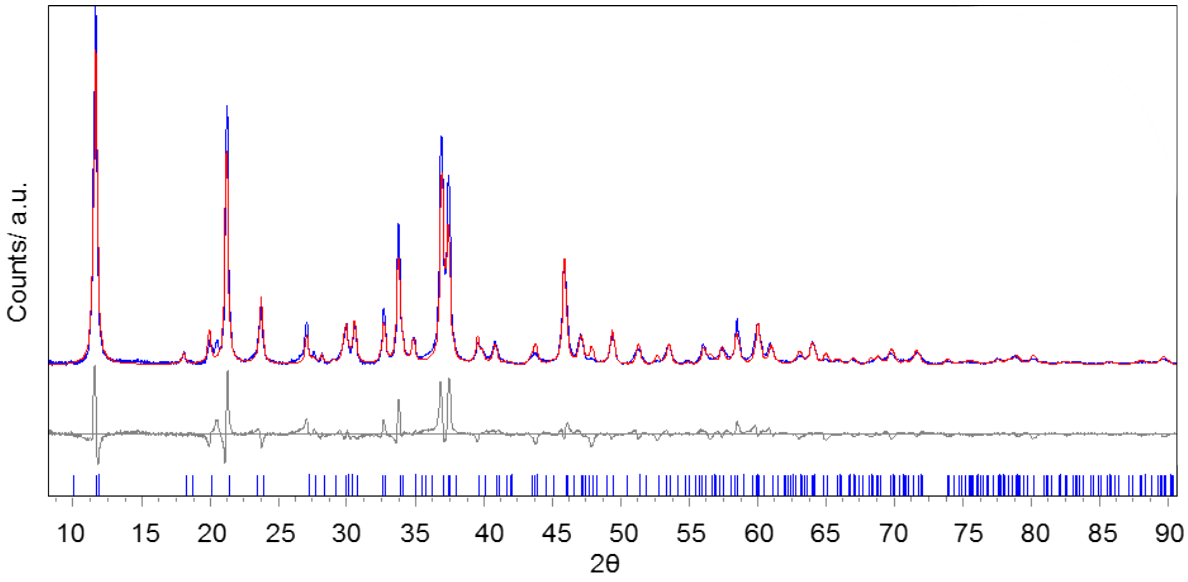

Figure S5. Rietveld refinement of the XRD pattern shown in Figure 3c. This sample contains 100 % $Mg_3(OH)_5Cl\ 4H_2O$. Tick marks correspond to 2θ position of diffraction peaks for F5 phase of magnesium oxychloride.